

Optimal Flow Control and Topology Optimization Using the Continuous Adjoint Method in Unsteady Flows

Ioannis S. Kavvadias, George K. Karpouzas, Evangelos M. Papoutsis-Kiachagias, Dimitris I. Papadimitriou, Kyriakos C. Giannakoglou

Abstract This paper presents the development and application of the unsteady continuous adjoint method to the incompressible Navier–Stokes equations and its use in two different optimization problems. The first is the computation of the optimal setting of a flow control system, based on pulsating jets located along the surface of a square cylinder, in order to minimize the time-averaged drag. The second is dealing with unsteady topology optimization of a duct system with four fixed inlets and a single outlet, with periodic in time inlet velocity profiles, where the target is to minimize the time-averaged viscous losses. The presentation of the adjoint formulation is kept as general as possible and can thus be used to other optimization problems governed by the unsteady Navier–Stokes equations. Though in the examined problems the flow is laminar, the extension to turbulent flows is doable.

1 Introduction

Adjoint methods [1, 2, 3, 4] are successfully used to compute the gradient of the objective function with respect to the design variables and support gradient-based optimization methods. This paper is dealing with the unsteady continuous adjoint [5, 6, 7, 8] methods, where the adjoint PDEs are firstly derived and, then, discretized. The primal problem is governed by the unsteady flow equations and time-averaged performance metrics are used as objective functions. Two optimization problems are solved: an active flow control and a topology optimization problem.

Ioannis S. Kavvadias, George K. Karpouzas, Evangelos M. Papoutsis-Kiachagias, Dimitris I. Papadimitriou, Kyriakos C. Giannakoglou
National Technical University of Athens (NTUA), School of Mechanical Engineering, Parallel CFD & Optimization Unit, Lab. of Thermal Turbomachines, Iroon Polytechniou 9, Athens 15780, Greece, e-mail: kavvadiasj@hotmail.com, grgkarpou@yahoo.gr, vaggelisp@gmail.com, dpapadim@mail.ntua.gr, kgianna@central.ntua.gr

Active flow control [9, 10], based on suction of blowing jets, steady or unsteady, may control the boundary layer of the flow by preventing or delaying separation or controlling other flow phenomena, such as the Karman vortices generated behind a cylinder. The case examined here is the unsteady flow developed around a square cylinder, which is controlled by a set of pulsating jets at fixed locations around the cylinder, with their amplitudes as the design variables.

On the other hand, topology optimization is a shape parameterization-free design method, which is used to identify which parts of an extended domain should be solidified, so as to minimize the objective function which quantifies the quality of the fluid flow in the remaining, non-solidified, part of the domain. Two major variances of topology optimization exists, the porosity [11, 12, 13] and the level-set [14, 15] methods.

The porosity-based class of topology optimization algorithms compute a real-valued porosity field, a , over an extended domain, which minimizes the objective function. Domain areas corresponding to the fluid flow are identified as those with nodal values $a = 0$ or, practically, $a \leq \varepsilon$ where ε is an infinitesimally small positive number. Remaining areas where $a \neq 0$ or, practically, $a > \varepsilon$ define the part of the domain to be solidified. In contrast, the level-set method is based on the signed distance φ from the sought solid-fluid interface. If locally $\varphi < 0$, this cell is a fluid cell, whereas cells with $\varphi > 0$ must be solidified. The isolines $\varphi = 0$ define the solid walls.

In this paper, the topology optimization is based on the level-set method and aims at designing a duct system with four fixed inlets and a single fixed outlet, for minimum time-averaged viscous losses. Unsteadiness is caused by the time-varying inlet velocity profiles.

In the unsteady adjoint method, a major issue is the storage of the primal solution fields, at different time steps. When solving the unsteady adjoint equations, information travels backwards in time. Also, to solve the adjoint equations at a given time instant, the primal fields for the same instant must be available. The full-storage of the primal field evolution in time is memory-wise too expensive and alternatives must be used. The check-pointing technique [16, 17], which is used in this paper, stores the primal solution at a number of instants and recomputes the solution at all other time instants, starting from the closest check-point.

2 Flow Model and Objective Functions

The flow is modeled by the Navier–Stokes equations for the unsteady laminar flow of an incompressible fluid. The last term in eq. 1, which is activated only in topology optimization problems, is added. The primal equations are

$$R_i^v = \frac{\partial v_i}{\partial t} + v_j \frac{\partial v_i}{\partial x_j} - \frac{\partial}{\partial x_j} \left[v \left(\frac{\partial v_i}{\partial x_j} + \frac{\partial v_j}{\partial x_i} \right) \right] + \frac{\partial p}{\partial x_i} + \alpha H(\varphi) v_i = 0, \quad i = 1, 2(3) \quad (1)$$

$$R^p = -\frac{\partial v_j}{\partial x_j} = 0 \quad (2)$$

where v_i and p stand for the velocity components and the static pressure divided by the density, respectively. φ is the signed distance (d or $-d$) from the solid walls used in the level set method,

$$\varphi(x) = \begin{cases} d & , \text{ if } x \in \text{solid region } (\Omega_s), \\ -d & , \text{ if } x \in \text{fluidic region } (\Omega_f), \\ 0 & , \text{ if } x \text{ is on the interface.} \end{cases} \quad (3)$$

$H(\varphi)$ is the Heaviside function and α is a penalty multiplier.

In view of the derivation of the primal equations, needed for the adjoint equations, the non-differentiable Heaviside function is replaced with the sigmoid function

$$\widehat{H}(\varphi, h) = \begin{cases} 1 & , \text{ if } \varphi \geq h \\ \frac{1}{2} + \frac{15\varphi}{16h} - \frac{5\varphi^3}{8h^3} + \frac{3\varphi^5}{16h^5} & , \text{ if } |\varphi| < h \\ 0 & , \text{ if } \varphi \leq -h \end{cases}$$

and its derivative is

$$\tau(\varphi, h) = \frac{\partial \widehat{H}(\varphi, h)}{\partial \varphi} = \begin{cases} +\frac{15}{16h} \left(1 - \frac{\varphi^2}{h^2} \right) & , \text{ if } |\varphi| < h \\ 0 & , \text{ if } |\varphi| \geq h \end{cases}$$

where h takes on a very small positive value determining the shape of the sigmoid function.

For the numerical solution of the primal equations the SIMPLE algorithm [18] was used, with a cell-centered, finite-volume discretization scheme.

The first problem examined is the design of an optimal flow control system. It is about the optimal configuration of a set of pulsating jets activated at fixed locations along the perimeter of a square cylinder, to minimize the time-averaged drag. The velocity components of each jet are given by

$$v_\lambda^m = (A^m \sin(2\pi f^m (t - f_0^m)) - A^m) n_\lambda, \quad \lambda = 1, 2(3) \quad (4)$$

where m is the jet counter. A^m is the amplitude, f^m the frequency and f_0^m the phase of each jet. Jets are aligned with the outwards, normal to the wall, unit vector. Positive A^m corresponds to blowing and negative A^m to suction. The frequencies f^m and phases f_0^m of all jets are the same and fixed to $f^m = \frac{v_\infty}{d}$ [8] and $f_0^m = 0$, where v_∞ is the infinite flow velocity and d is the side length of the square cylinder. The only design variables are the amplitudes A^m . In this case, the period of pulsating jets is about 6 times shorter than that of the Karman vortices.

The time-averaged (squared) drag force is expressed as

$$J_1 = \frac{1}{2T} \int_T D^2(t) dt \quad (5)$$

where T is the flow period. In the uncontrolled case, the flow period is the Karman vortices' period whereas in the optimally controlled case T stands for the jets' period. D is the time-dependent drag force

$$D(t) = \int_{S_w} \left[pn_i - v \left(\frac{\partial v_i}{\partial x_j} + \frac{\partial v_j}{\partial x_i} \right) n_j - |v_j n_j| v_i \right] r_i dS \quad (6)$$

where r_i are the components of the unit vector aligned with the farfield velocity and S_w stands for the solid wall boundary. The last term in eq. 6 stands for the contribution of jets on the forces acting upon the body, at the jets locations. A similar study, for a circular cylinder, can be found in [8].

The second problem is concerned with the design of an optimal duct system connection fixed inlets with a single outlet. The flow is unsteady since time-varying inflow conditions are imposed. The velocity at each inlet is still given by eq. 4, where $A^m(> 0)$, f^m and f_0^m have fixed values. The problem is handled as a topology optimization problem on an extended domain where the level set values φ at each cell center are the design variables.

The objective function to be minimized is the time- and mass-averaged total pressure losses between the inlets S_I and the outlet S_O . This is mathematically expressed as

$$J_{p_t} = -\frac{1}{T} \int_T \int_{S_I, O} \left(p + \frac{1}{2} v_j v_j \right) v_i n_i dS dt \quad (7)$$

with a term expressing a volume constraint being added to it. The constraint function is

$$c = \left[\frac{\int_{\Omega} H(\varphi) d\Omega}{V_{all}} - V_{tar} \right]^2 = \left(\frac{V_{solid}}{V_{all}} - V_{tar} \right)^2 \quad (8)$$

where V_{all} is the volume of Ω , V is the volume occupied by fluid, V_{solid} that of the solidified part of the domain and V_{tar} gives the desired percentage of Ω to be solidified. After including the equality constraint of eq. 8, the objective function becomes

$$J_2 = J_{p_t} - \lambda c + w c^2 \quad (9)$$

where λ is a Lagrangian multiplier and w a weight associated with the constraint. During the optimization loop, both are updated according to the Augmented Lagrange Multiplier (ALM) algorithm [19]. λ is initialized with a zero value and w with a small positive value. At the end of each optimization cycle, w is multiplied by a user-defined positive factor $\gamma > 1$ (unless it exceeds w_{max}) and λ is updated as $\lambda^{new} = \lambda^{old} - 2w^{old}c$.

3 The Continuous Unsteady Adjoint Method

3.1 Field Adjoint Equations

The augmented objective function L_k is defined as the sum of J_k and the time-space $(T - \Omega)$ integrals of the products of the state equations and the corresponding adjoint fields. So,

$$L_k = J_k + \int_T \int_{\Omega} u_i R_i^v d\Omega dt + \int_T \int_{\Omega} q R^p d\Omega dt, \quad k = 1, 2 \quad (10)$$

where u_i and q are the adjoint velocities and pressure, respectively.

The derivatives of L_k w. r. t. the design variables b_m , after applying the Leibniz theorem, become

$$\frac{\delta L_k}{\delta b_m} = \frac{\delta J_k}{\delta b_m} + \int_T \int_{\Omega} u_i \frac{\partial R_i^v}{\partial b_m} d\Omega dt + \int_T \int_{\Omega} q \frac{\partial R^p}{\partial b_m} d\Omega dt \quad (11)$$

By applying the Green-Gauss theorem and eliminating the integrals which depend on variations in the flow variables w. r. t. b_m , the field adjoint equations are derived. These are

$$R^q = \frac{\partial u_i}{\partial x_i} = 0 \quad (12)$$

$$R_i^u = -\frac{\partial u_i}{\partial t} - v_j \frac{\partial u_i}{\partial x_j} + u_j \frac{\partial v_j}{\partial x_i} + \frac{\partial q}{\partial x_i} - \frac{\partial}{\partial x_j} \left[v \left(\frac{\partial u_i}{\partial x_j} + \frac{\partial u_j}{\partial x_i} \right) \right] + \alpha H(\varphi) u_i = 0 \quad (13)$$

Since both objective functions, J_1 and J_{pt} , comprise only boundary integrals, their derivatives $\frac{\delta J_1}{\delta b_m}$ and $\frac{\delta J_{pt}}{\delta b_m}$ are defined only at these boundaries and do not contribute to the adjoint field equations. The c constraint term, added to J_{pt} to form J_2 , contains a volume integral which contributes only to the sensitivity derivatives. Since none of the objective functions contributes to the field adjoint equations, the same field adjoint equations are valid for both. Of course, in the flow control optimization problem, the last term in eq. 13 vanishes.

After eliminating the integrals depending on the variations in flow quantities, the sensitivity derivatives are expressed, in the most general form, as

$$\begin{aligned} \frac{\delta L_k}{\delta b_m} &= \frac{\delta J_k}{\delta b_m} + \int_{\Omega} \left[v_i \frac{\partial v_i}{\partial b_m} \right]_0 d\Omega + \int_T \int_S D_i^u \frac{\partial v_i}{\partial b_m} dS dt + \int_T \int_S D^q \frac{\partial p}{\partial b_m} dS dt \\ &+ \int_T \int_S E_i^u \left[\frac{\partial}{\partial x_j} \left(\frac{\partial v_i}{\partial b_m} \right) + \frac{\partial}{\partial x_i} \left(\frac{\partial v_j}{\partial b_m} \right) \right] n_j dS dt \end{aligned} \quad (14)$$

where $S = S_I \cup S_O \cup S_w$ or $S = S_{\infty} \cup S_w$ is the boundary and $D_i^u = u_i v_j n_j + v \left(\frac{\partial u_i}{\partial x_j} + \frac{\partial u_j}{\partial x_i} \right) n_j - q n_i$, $E_i^u = -v u_i$ and $D^q = u_j n_j$.

By substituting the derivative of each objective function into eq. 14, the elimination of the boundary integrals which depend on the variation in the flow variables gives the adjoint boundary conditions. The remaining terms give the expression of the sensitivity derivatives to be used in the descent algorithm.

3.2 Boundary Conditions & Sensitivity Derivatives for J_1

The derivative of the 'mean drag' objective function w. r. t. b_m is

$$\begin{aligned} \frac{\delta J_1}{\delta b_m} = & \frac{1}{T} \int_T \int_{S_w} D \left(-\mathbf{v} \left[\frac{\partial}{\partial x_j} \left(\frac{\partial v_i}{\partial b_m} \right) + \frac{\partial}{\partial x_i} \left(\frac{\partial v_j}{\partial b_m} \right) \right] n_j \right. \\ & \left. + \frac{\partial v_i}{\partial b_m} |v_j n_j| + \frac{v_j n_j}{|v_j n_j|} \frac{\partial v_j}{\partial b_m} n_j v_i + \frac{\partial p}{\partial b_m} n_i \right) r_i dS dt \end{aligned} \quad (15)$$

After substituting eq. 15 into eq. 14, the elimination of the boundary integrals depending on the variation of the flow variables w. r. t. b_m gives the adjoint boundary conditions at every time step.

The adjoint boundary conditions along S_w , S_I and S_O , at every time-step, are S_w : $u_i = -\frac{D(t)}{T} r_i$ and S_{∞} : $u_i = 0$; for the whole domain Ω , the initial condition at $t = T$ is $u_i|_{t=T} = 0$.

The incoming or outgoing adjoint velocity is proportional to the instantaneous value of drag $D(t)$; this is the origin of the unsteady adjoint flow.

Finally, the sensitivities of J_1 w. r. t. the control variables $b_m = A^m$ are given by

$$\begin{aligned} \frac{\delta J_1}{\delta b_m} = & \int_T \int_{S_w} \left[u_i v_j n_j - u_i |v_j n_j| + \mathbf{v} \left(\frac{\partial u_i}{\partial x_j} + \frac{\partial u_j}{\partial x_i} \right) n_j \right. \\ & \left. - q n_i - \frac{v_j n_j}{|v_j n_j|} u_j v_j n_i \right] (\sin(2\pi f^m(t - f_0^m)) - 1) n_i dS dt \end{aligned} \quad (16)$$

3.3 Boundary Conditions & Sensitivity Derivatives for J_2

For the time-averaged total pressure losses, used in topology optimization, the adjoint boundary conditions are derived by substituting the derivative of J_2 w. r. t. b_m in eq. 14 and eliminating terms depending on the derivatives of the flow fields. The derivative of J_2 w. r. t. b_m is

$$\begin{aligned} \frac{\delta J_2}{\delta b_m} = & -\frac{2}{T} \int_T \int_{S_{I,O}} \left[v_i n_i \frac{\partial p}{\partial b_m} + \left(v_i v_j n_j + \left(p + \frac{1}{2} v_j^2 \right) \right) \frac{\partial v_i}{\partial b_m} \right] dS dt \\ & + (4wc - \lambda) \left(\frac{V_{solid}}{V_{all}} - V_{tar} \right) \frac{\int_{\Omega} \tau(\varphi) d\Omega}{V_{all}} \end{aligned} \quad (17)$$

The adjoint boundary conditions are $S_w: u_i = 0$, $S_I: u_{(n)} = \frac{v_{(n)}}{T}$, $u_{(t)} = 0$, $S_O: q = u_{(n)}v_{(n)} + v \left(\frac{\partial u_{(n)}}{\partial n} + \frac{\partial u_{(n)}}{\partial t} \right) + (p + \frac{1}{2}v^2) + v_{(n)}v_{(n)}$ and $u_{(t)}v_{(n)} + v \left(\frac{\partial u_{(t)}}{\partial n} + \frac{\partial u_{(n)}}{\partial t} \right) + v_{(t)}v_{(n)} = 0$ and the initial condition for the adjoint field, at $t = T$, is $u_i|_{t=T} = 0$. The indices (n) and (t) stand for the normal and tangent components to the boundary.

The sensitivity derivatives of J_2 w. r. t. b_m , where b_m are the φ values at the cell-center, are

$$\frac{\delta J_2}{\delta b_m} = \frac{\delta J_2}{\delta \varphi} = \int_{\Omega} [\alpha (v_i u_i) \tau(\varphi)] d\Omega + 2(-\lambda + 2wc) \left(\frac{V_{solid}}{V_{all}} - V_{tar} \right) \frac{\int_{\Omega} \tau(\varphi) d\Omega}{V_{all}} \quad (18)$$

3.4 Check-pointing

For the solution of the unsteady adjoint equations, the primal fields at all time steps must be available. Since the adjoint information travels backwards in time, in order to use the primal fields at each time step, these should have been stored during the solution of the primal equations. Due to memory limitations, this is replaced by the binomial check-pointing technique.

The check-pointing technique is a compromise between memory consumption and CPU cost. Instead of storing the primal solutions at every time step, which is very memory consuming, only those at a predefined number of time-instances, called check-points, are stored; from them, the primal solution in every other time-instant is re-computed.

The binomial check-pointing method uses a binomial distribution of check-points in time, for which it can be proved [17] that the number of flowfield recomputations is minimal for given numbers of check-points and time-steps. The distribution of check-points is dynamically updated as time progresses, so that, at any given time-step, each check-point is always in the optimal position in time, as dictated by the binomial distribution.

4 Results

In both optimization problems, the steepest descent method [19]

$$b_m^{new} = b_m^{old} - \eta \frac{\delta J_k}{\delta b_m} \quad (19)$$

is used to update the design variables values, after solving the adjoint equations.

4.1 Flow Control Optimization

The Reynolds number of the flow around the cylinder is $Re=100$. Five jets were equi-distributed along each side of the square cylinder, the placement of which can be seen in fig. 5. All 20 jets share the same frequency $f^m = v_\infty/d = 10Hz$ and phase $f_0^m = 0$. Recall that the optimization variables are the amplitudes A^m of the jets and the minimization of J_1 is targeted.

The time step for the simulation is $\Delta t = 4 \cdot 10^{-4}$. Two variants were tried. In the first variant, the so-called "full-in-time" approach, the flow computation was performed for 11 periods of time in each optimization cycle. It was decided to discard the solution during the first 5 periods, so as to get rid of the transient phase of the primal problem and do the same for the last 5 to also avoid the transient phase of the adjoint problem. Only the intermediate period, which is considered representative of the periodic primal and adjoint phenomena, was used to calculate sensitivity derivatives and the value of the objective function. In the second variant, to be referred to as the "fast-in-time" approach, only one period of time is simulated in each optimization cycle. After the numerical solution of the primal equations for a single period of time, the adjoint equations were solved for this period. Then, the sensitivity derivatives were computed using the solution to the primal and adjoint equations, for this single period, and the design variables were updated.

Because the transient effects were not discarded, the computed sensitivities were not exact but the CPU cost per optimization cycle was lower. In order to reduce transient effects, the results at the last time-step of the previous period/cycle were used as initialization for the primal flow in the next optimization cycle. For the adjoint equations, the first time-instant was used instead, since time goes backwards. At the end of the optimization process, both the primal and the adjoint equations were converged to a periodic solution.

In this case, 400 check-points were used and enough optimization cycles were performed for both variants to converge. The convergence of both approaches is presented in fig. 1. The "fast-in-time" simulation appears to be twice as fast as the "full-in-time" one. As such, the "fast-in-time" approach was exclusively used in the second problem.

As both variants converged to a similar mean drag value and, except convergence, only the outcome of the "fast-in-time" approach is shown.

The time variation in the drag and lift coefficients for the uncontrolled and controlled cases are shown in figs. 3 and 4. The resulted reduction in the amplitude of the oscillating lift force is nothing more than a by-product of the optimization process and is attributed to the controlled flow field symmetry.

A snapshot of the optimized flow, at an arbitrary time instant, is presented in fig. 5. The Karman vortices of the uncontrolled flow were suppressed and both the primal and adjoint flows are symmetric in space. Also, the wake in the adjoint flow, developed in the upwind direction, is visible.

The computed optimal jet amplitudes are shown in fig. 2. Slots 4 to 10 create symmetric vortices above and below the cylinder and slots 1 to 3 push them away.

These vortices do not allow the Karman street to be developed and produce a symmetric flow field around the horizontal axis.

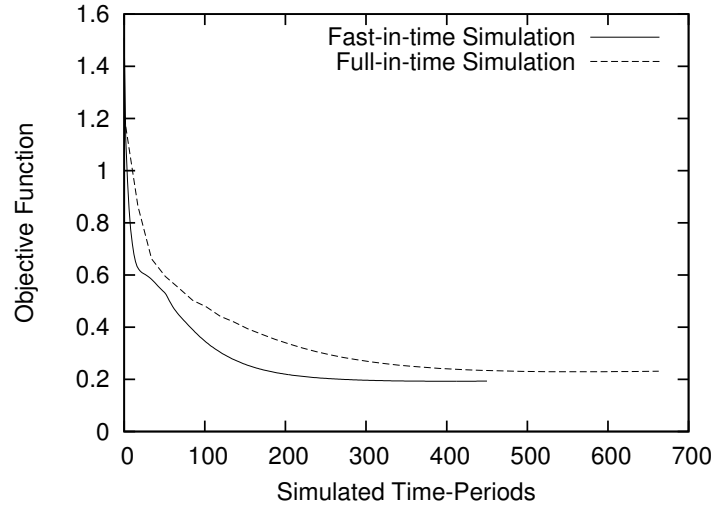


Fig. 1 Flow control optimization - mean drag minimization of a square cylinder, at $Re = 100$. Convergence of both “-in-time” approaches. The x-axis corresponds to simulated periods of time. For the “full-in-time” approach, each optimization cycle solves 11 primal and 6 adjoint periods, while the “fast-in-time” approach solves for only 1 primal and 1 adjoint period per cycle. From this case, a speed-up of about $\times 2$ was achieved by using the “fast-in-time” approach.

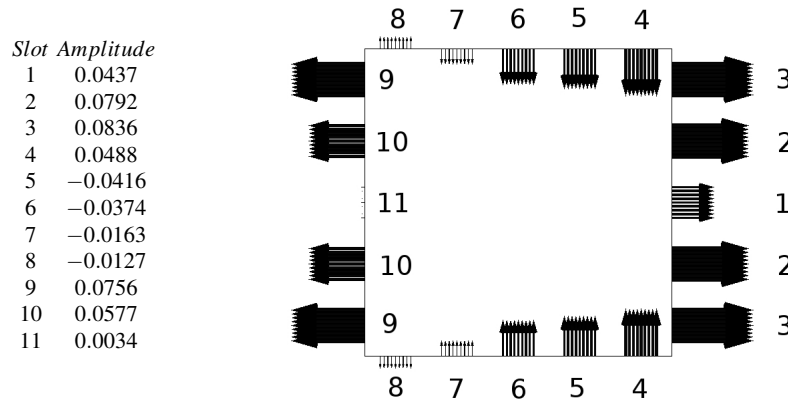


Fig. 2 Flow control optimization - mean drag minimization of a square cylinder, at $Re = 100$. Jet locations and slot widths are shown. The computed optimal amplitudes of the pulsating jets are listed and sketched.

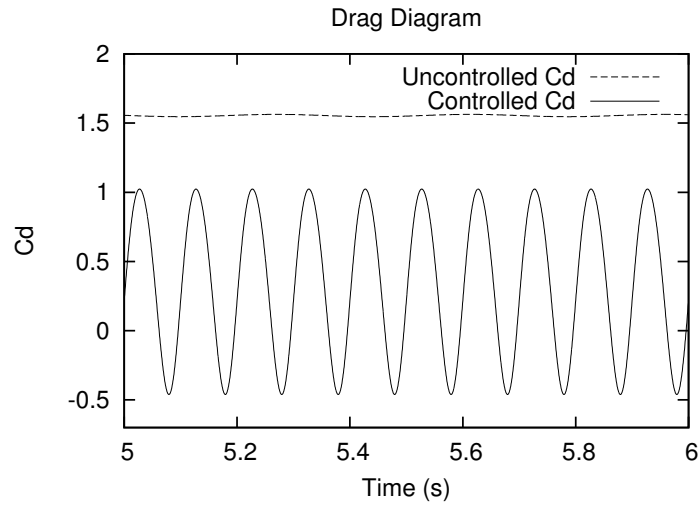


Fig. 3 Flow control optimization - mean drag minimization of a square cylinder, at $Re = 100$. Drag coefficient $C_d (= \frac{D(t)}{0.5d^2v_\infty^2})$ for the uncontrolled case and the optimally controlled configuration. The mean drag coefficient was reduced from ~ 1.6 to ~ 0.3 .

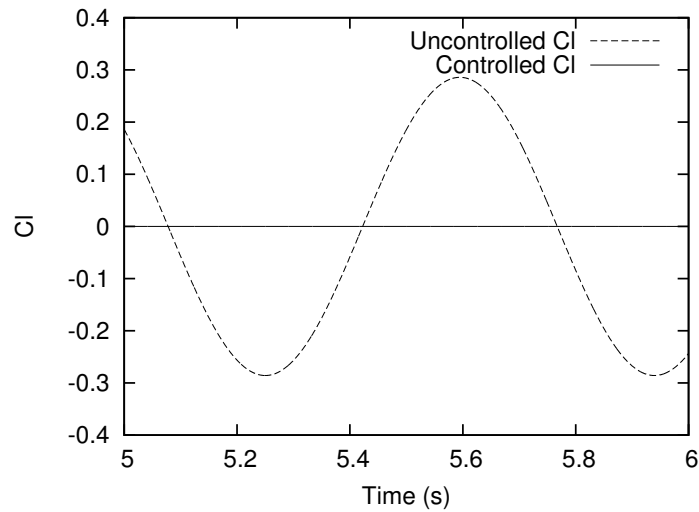


Fig. 4 Flow control optimization - mean drag minimization of a square cylinder, at $Re = 100$. Lift coefficient C_l for the uncontrolled and the optimally controlled configuration. The lift was almost stabilized to zero, though this was not included in the objective function.

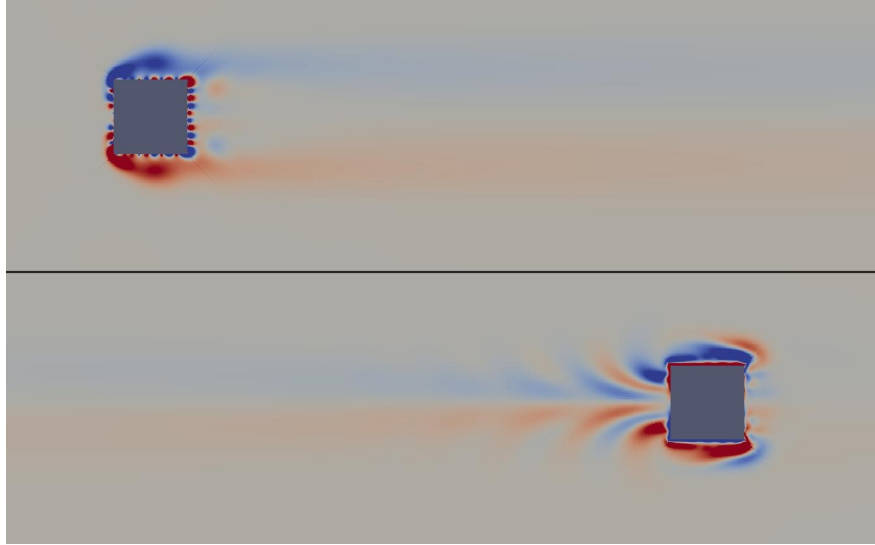


Fig. 5 Flow control optimization - mean drag minimization of a square cylinder at $Re = 100$. The optimal solution is shown. Snapshot of the vorticity field at a random time instant. Primal (top) and adjoint (bottom) vorticity fields.

4.2 Unsteady Topology Optimization

The topology optimization was carried out on an empty square box, $2m \times 2m$, with four inlets of $5cm$ each and a single $15cm$ outlet. The set-up of the inlets and outlets is shown in fig. 6. The velocity at each inlet is expressed by eq. 4. All inlet velocity profiles share the same amplitude $A^m = 1m/s$ and frequency $f^m = 10Hz$, but each had each own phase, $f_0^1 = 0.05$, $f_0^2 = 0$, $f_0^3 = 0.075$ and $f_0^4 = 0.025$. The percentage of the square box volume to be solidified was initially set at 60% or, in eq. 8, $V_{tar} = 0.6$. For the sake of comparison, a second optimization was carried out using $V_{tar} = 0.8$. The target is to minimize J_2 .

In this case, only the "fast-in-time" approach was used.

The optimal shape of the duct, for each constraint, is shown in fig. 6 and the progress of the optimization algorithm in fig. 7. Also, four snapshots of the velocity field are presented in fig. 8, for $V_{tar} = 0.6$, each corresponding to the time instant at which the velocity of each inlet jet is at its maximum value.

5 Conclusions

The development of the unsteady continuous adjoint method to the incompressible Navier–Stokes equations was presented for two optimization problems. The first is a flow control optimization, using pulsating jets, of the unsteady flow around a square

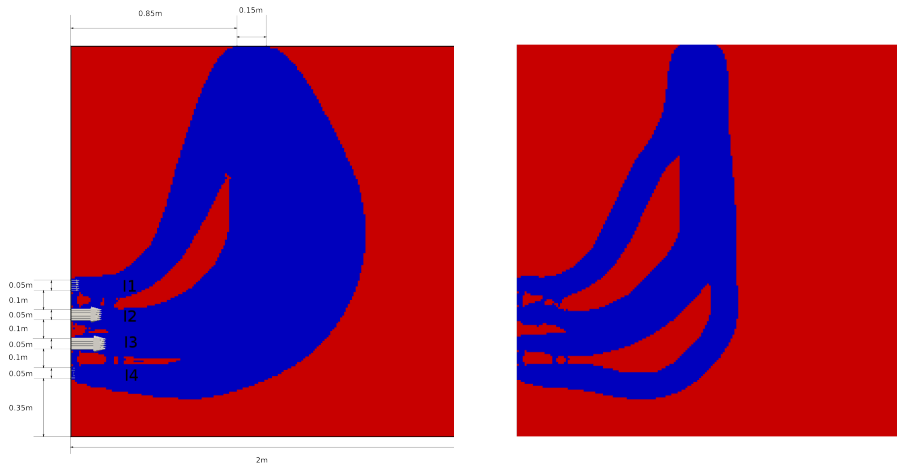


Fig. 6 Unsteady Topology Optimization. The $\hat{H}(\varphi)$ field showing the optimal duct computed by the optimization loop. Left: $V_{tar} = 0.6$, Right: $V_{tar} = 0.8$, Red areas ($\hat{H}(\varphi) \approx 1$) indicate the solidified part of the domain whereas the blue one ($\hat{H}(\varphi) \approx 0$) is the fluid. Left: the inlet velocity vectors at this instant are also shown, so as to make clear that the four incoming mass flow rates are not in phase.

cylinder and the second is a level-set optimization problem to design an optimal duct system in a box with four inlets, a single outlet and unsteady inlet boundary conditions, under a volume constraint.

On the flow control problem the optimal amplitude for each jet, as well as its type (blowing or suction) were identified. On the topology optimization problem, the optimal duct systems were identified for different volume constraints, based on the level-set optimization method.

In all cases, the binomial check-pointing method was used to overcome the memory requirements of the unsteady adjoint method.

The "fast-in-time" technique was formulated, where the optimization is based on an approximation of the sensitivity derivatives, due to transient effects. Using this technique, though more optimization cycles are needed, each one of them is much cheaper in CPU cost and the over-all time needed by the "fast-in-time" technique is about half the time needed by its "standard" counterpart.

References

1. Pironneau, O. On optimum design in fluid mechanics. *Journal of Fluid Mechanics* **64**, 97–110 (1974).
2. Jameson, A. Aerodynamic design via control theory. *Journal of Scientific Computing* **3**, 233–260 (1988).

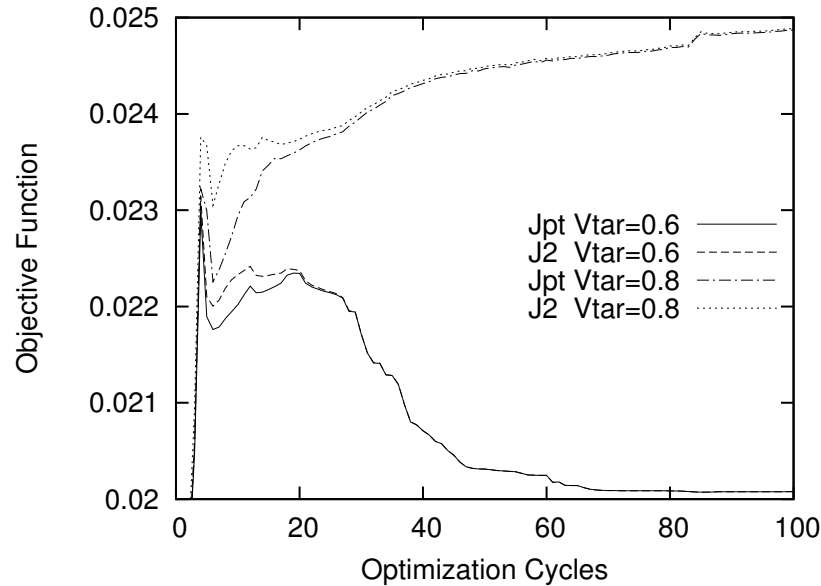


Fig. 7 Unsteady Topology Optimization. The mean total pressure losses as the optimization algorithm progresses. The presented results correspond to two runs with different constraints, $V_{tar} = 0.6$ and $V_{tar} = 0.8$. The number of optimization cycles might appear to be high but the CPU cost per cycle is quite low since both the primal and adjoint equations were solved for a single period of time only. The constrained and unconstrained value of the objective function are plotted. Once the solidified part of the domain reaches the desired percentage of the overall volume, the terms added to J_p become zero and the two curves coincide. As expected, increasing the solidified part of the domain led to a narrow fluid passage and increased pressure losses.

- Shubin, G. and Frank, P. A comparison of the implicit gradient approach and the variational approach to aerodynamic design optimization. *Boeing Computer Services Report AMS-TR-163* (1991).
- Burgreen, G. and Baysal, O. Three-dimensional aerodynamic shape optimization using discrete sensitivity analysis. *AIAA Journal* **34**(9), 1761–1770 (1996).
- Anderson, W. and Venkatakrishnan, V. Aerodynamic design optimization on unstructured grids with a continuous adjoint formulation. In *35th Aerospace Sciences Meeting and Exhibit* (, Reno, NV, USA, 1997). AIAA-1997-0643.
- Papadimitriou, D. and Giannakoglou, K. Aerodynamic shape optimization using first and second order adjoint and direct approaches. *Archives of Computational Methods in Engineering (State of the Art Reviews)* **15**(4), 447–488 (2008).
- Wang, Q. *Uncertainty Quantification for Unsteady Fluid Flow Using Adjoint-Based Approaches*. PhD thesis, Stanford, USA, (2008).
- Carnarius, A., Thiele, F., E., O., Nemili, A., and Gauger, N. Optimal control of unsteady flows using a discrete and a continuous adjoint approach. *System Modeling and Optimization, IFIP Advances in Information and Communication Technology* **391**, 318–327 (2011).
- Bewley, T. Flow control: new challenges for a new renaissance. *Progress in Aerospace Sciences* **37**, 21–58 (2001).
- Zymaris, A., Papadimitriou, D., Papoutsis-Kiachagias, E. M., Giannakoglou, K., and Othmer, C. The continuous adjoint method as a guide for the design of flow control systems based on jets. *Engineering Computations* **30**(4) (2013).

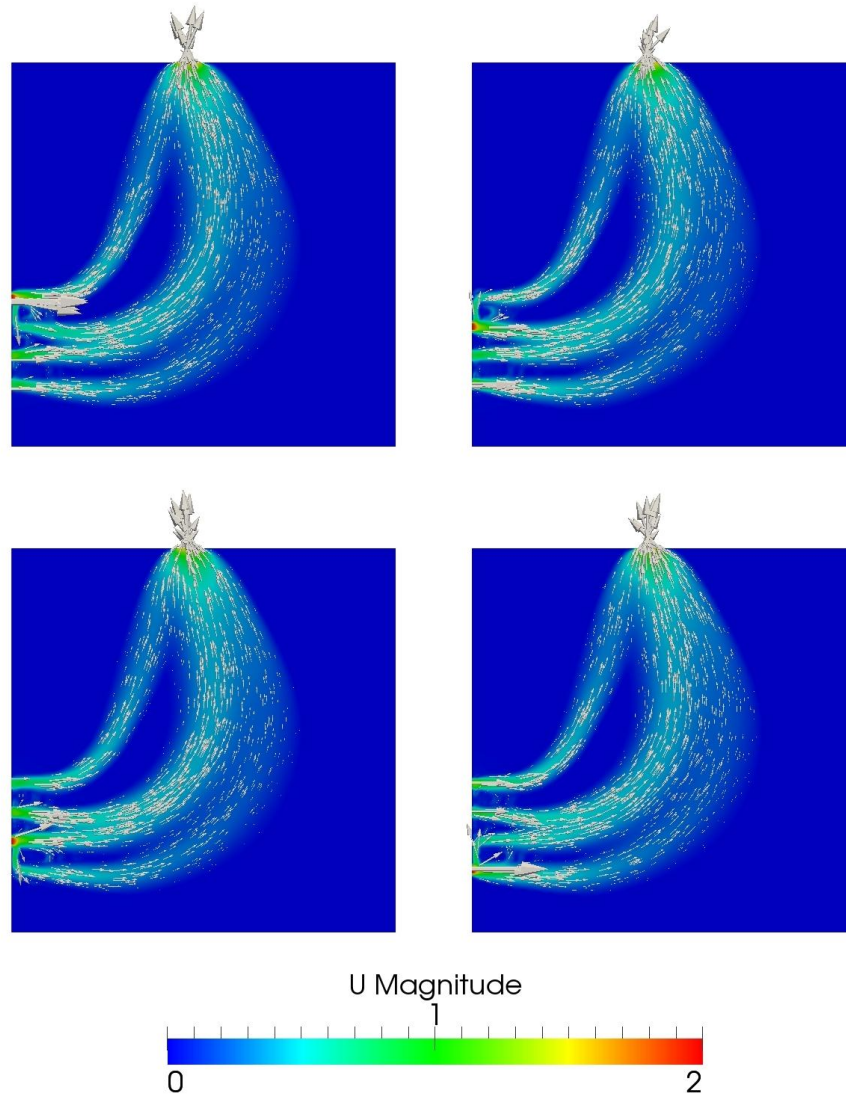


Fig. 8 Unsteady Topology Optimization. The velocity flow field at 4 different time instants, corresponding to maximum velocities at inlet 1 (top-left), inlet 2 (top-right), inlet 3 (bottom-left) and inlet 4 (bottom-right). Strong swirl effects are present close to the flow outlet. Should these be undesirable, they could be controlled or even eliminated [13] by adding a second constraint to the objective function.

11. Borvall, T. and Peterson, J. Topology optimization of fluids in stokes flow. *International Journal for Numerical Methods in Fluids* **41**, 77–107 (2003).
12. Gersborg-Hansen, A., Sigmund, O., and Haber, R. Topology optimization of channel flow problems. *Structural and Multidisciplinary Optimization* **30**, 181–192 (2005).
13. Kontoleonos, E. A., Papoutsis-Kiachagias, E. M., Zymaris, A. S., Papadimitriou, D. I., and Giannakoglou, K. C. Adjoint-based constrained topology optimization for viscous flows, including heat transfer. *Engineering Optimization* **45(8)**, 941–961 (2013).
14. Sethian, J. Evolution, implementation, and application of level set and fast marching methods for advancing fronts. *Journal of Computational Physics* **169**, 503–555 (2001).
15. Chang, Y., Hou, T., Merriman, B., and Osher, S. A level set formulation of eulerian interface capturing methods for incompressible fluid flows. *Journal of Computational Physics* **124**, 449–494 (1996).
16. Griewank, A. and Walther, A. Algorithm 799: revolve: an implementation of checkpointing for the reverse or adjoint mode of computational differentiation. *ACM Transactions on Mathematical Software (TOMS)* **26(1)**, 19–45 (2000).
17. Wang, Q., Moin, P., and Iaccarino, G. Minimal repetition dynamic checkpointing algorithm for unsteady adjoint calculation. *SIAM Journal on Scientific Computing* **31(4)**, 25492567 (2008).
18. Caretto, L., Gosman, A., Patankar, S., and Spalding, D. Two calculation procedures for steady three-dimensional flows with recirculation. In *Proceedings of the Third International Conference on Numerical Methods in Fluid Mechanics* (, Paris, 1972).
19. Nocedal, J. and Wright, S. *Numerical Optimization*. Springer, (1999).